High Frequency of Urban New Particle Formation on the Tibetan Plateau: Quantifying Formation Rates, Growth Rates, and CCN Production

Qiqi Mo[1], Longjie Wen[1,2], Gang Zhao[1,3*], Chunxiang Ye[4*], Jie Sun[1], Weili Lin[1,5], Fengjun Shen[1], Tong Liu[1], Yicheng Gao[1], Yi Chen[4], Tiantian Zhang[1], Tong Zhu[4]

[1]Key Laboratory of Ecology and Environment in Minority Areas, Minzu University of China, National Ethnic Affairs Commission, Beijing 100081, China
[2]School of Ecology and Environment, College of Intelligence, Harbin Institute of Technology (Shenzhen), Shenzhen, 518055, China
[3]Key Laboratory of Biodiversity and Environment on the Qinghai-Tibet Plateau, Ministry of Education, Xizang University, Lhasa 850000, China
[4]SKL-ESPC & SEPKL-AERM, College of Environmental Sciences and Engineering, Institute of Tibetan Plateau, and Center for Environment and Health, Peking University, Beijing, China
[5]Institute of National Security, Minzu University of China, Beijing, 100081, China

Correspondence to: Gang Zhao (gangz@muc.edu.cn) and Chunxiang Ye (c.ye@pku.edu.cn)

Section S1

Table S1

Figure S1 to Figure S8

Section S1 Calculation of the H_2SO_4-related photochemical proxy

Because gaseous H_2SO_4 was not directly measured, a relative H_2SO_4-related photochemical proxy was calculated to examine the possible association between sulfur-containing precursor availability and new particle formation (NPF) during the autumn observation period. The proxy was based on the approximate balance between the photochemical production of H_2SO_4 through OH-initiated oxidation of SO_2 and its condensational loss to the pre-existing aerosol population (Petäjä et al., 2009; Dada et al., 2020):

$$P(H_2SO_4) = [SO_2]\, J(O(^1D))/CS \quad \text{(S1)}$$

where $[SO_2]$ is the molecular number concentration of SO_2, J(O(¹D)) is the O_3 photolysis frequency, and CS is the condensation sink. J(O(¹D)) was used as an indicator of daytime photochemical OH production because tropospheric OH concentrations are often closely related to solar ultraviolet radiation and O_3 photolysis (Rohrer and Berresheim, 2006). The proxy therefore represents the potential photochemical production of H_2SO_4 relative to its condensational loss.

The SO_2 mixing ratio was converted from ppb to molecular number concentration according to

$$[SO_2] = \chi(SO_2) \times 10^{-9} \times P/(k_B T) \times 10^{-6} \quad \text{(S2)}$$

where $\chi(SO_2)$ is the SO_2 mixing ratio in ppb, P is atmospheric pressure in Pa, T is air temperature in K, and k_β is the Boltzmann constant. A representative pressure of 650 hPa was used for the TU site, and the factor 10^{-6} converts molecules m^{-3} to molecules cm^{-3}.

SO_2, temperature, J(O(¹D)), and CS were synchronized and averaged to a common 30 min time resolution. Negative SO_2 values were excluded. Negative J(O(¹D)) values attributable to instrumental noise were set to zero, and periods with non-positive or missing CS were excluded. Missing spectral measurements were not interpolated. The proxy was therefore calculated only when concurrent valid measurements of all required variables were available.

The spectral measurements used to derive J(O(¹D)) were available only during part of the autumn observation period. Consequently, the proxy analysis does not provide continuous coverage of the entire autumn campaign and was not used to compare the autumn and spring observation periods. Undefined and Non-Event days were combined as non-NPF days for this supplementary comparison.

No site-specific empirical coefficient relating J(O(¹D)) to OH or relating the proxy to measured H_2SO_4 was available. Therefore, $P(H_2SO_4)$ was used only as a relative photochemical proxy and should not be interpreted as an absolute gas-phase H_2SO_4 concentration. The proxy also neglects other potential H_2SO_4 sources, such as stabilized Criegee intermediate chemistry, and losses associated with molecular clustering. These omitted pathways may be important, particularly in urban environments (Dada et al., 2020).

Table S1. Day-by-day revised classification, NPF timing, particle number characteristics, and candidate particle growth rates during the two observation periods. Mean $N_{3–25}$ and $N_{25–100}$ concentrations were calculated over 09:00–18:00 local time. Candidate $GR_{3–7}$ and $GR_{7–20}$ values were evaluated for every observation day by linear regression of automatically identified continuous modal trajectories. No R^2 threshold was applied. "NA" indicates that insufficient data or no sufficiently long and continuous trajectory was available.

Date	Revised classification	Original growth subgroup	NPF window	Mean $N_{3–25}$ (10^3 # cm^{-3})	Mean $N_{25–100}$ (10^3 # cm^{-3})	$GR_{3–7}$ window	$GR_{3–7}$ (nm h^{-1})	$GR_{7–20}$ window	$GR_{7–20}$ (nm h^{-1})
Oct 9, 2024	NPF day	Class II	8:40–14:30	17.0	5.0	08:42–09:12	4.3	09:17–14:27	1.6
Oct 10, 2024	NPF day	Class II	9:00–15:00	10.8	4.0	NA	NA	09:22–14:57	1.9
Oct 16, 2024	NPF day	Class I	9:00–21:00	19.2	8.5	09:02–09:32	3.9	09:37–17:57	0.9
Oct 17, 2024	NPF day	Class II	9:00–14:00	16.6	5.4	NA	NA	09:07–13:57	2.2
Oct 18, 2024	NPF day	Class II	8:40–14:30	16.1	5.0	08:42–09:27	3.5	09:32–14:27	1.4
Oct 19, 2024	NPF day	Class II	9:00–15:00	6.3	3.9	09:02–09:37	1.8	09:42–14:57	2.4
Oct 20, 2024	NPF day	Class II	9:00–18:00	21.3	6.2	09:02–13:07	0.2	09:42–17:52	1.3
Oct 22, 2024	NPF day	Class I	9:00–22:00	20.4	6.8	09:02–16:37	0.0	09:37–17:57	-0.4
Oct 23, 2024	NPF day	Class II	9:00–15:00	12.2	4.2	NA	NA	09:02–14:57	0.9
Oct 24, 2024	NPF day	Class I	9:00–23:00	12.0	4.7	09:02–09:32	5.3	09:37–17:57	0.5
Oct 25, 2024	NPF day	Class I	9:00–21:00	11.9	4.7	09:02–09:47	3.6	09:52–17:57	1.2
Oct 26, 2024	NPF day	Class I	9:30–23:00	12.1	3.2	09:32–13:52	0.1	10:07–17:57	1.1
Oct 27, 2024	NPF day	Class I	9:30–22:00	15.6	6.4	NA	NA	09:47–17:57	1.3
Oct 28, 2024	NPF day	Class I	9:00–24:00	16.7	5.9	NA	NA	09:22–17:57	1.1
Oct 29, 2024	NPF day	Class I	9:30–24:00	10.1	5.4	NA	NA	09:47–17:57	1.4
Oct 30, 2024	NPF day	Class I	9:30–24:00	8.3	4.3	NA	NA	09:52–17:57	1.1
Oct 31, 2024	NPF day	Class I	9:30–21:00	9.4	6.1	NA	NA	10:02–17:57	0.8

Date	Revised classification	Original growth subgroup	NPF window	Mean $N_{3–25}$ (10^3 # cm^{-3})	Mean $N_{25–100}$ (10^3 # cm^{-3})	$GR_{3–7}$ window	$GR_{3–7}$ (nm h^{-1})	$GR_{7–20}$ window	$GR_{7–20}$ (nm h^{-1})
Nov 1, 2024	NPF day	Class I	9:30–24:00	18.4	6.9	NA	NA	10:02–17:57	0.9
Nov 2, 2024	NPF day	Class I	9:00–24:00	19.2	7.2	09:02–09:32	5.2	09:37–17:57	1.2
Nov 3, 2024	NPF day	Class I	9:00–21:00	14.4	6.7	09:02–09:52	3.1	09:57–17:57	1.3
Nov 4, 2024	NPF day	Class II	12:00–16:00	4.9	3.5	NA	NA	12:02–15:57	3.3
Nov 7, 2024	NPF day	Class I	9:00–24:00	24.5	8.2	NA	NA	09:27–17:57	0.5
Nov 8, 2024	NPF day	Class I	9:30–24:00	16.7	8.3	NA	NA	09:52–17:57	0.7
Nov 9, 2024	NPF day	Class I	9:30–24:00	14.0	7.0	NA	NA	09:42–17:57	1.1
Nov 10, 2024	NPF day	Class I	9:30–24:00	10.5	5.1	NA	NA	10:02–17:57	1.3
Mar 25, 2025	NPF day	Class I	9:00–21:00	13.3	3.2	NA	NA	09:25–18:00	1.1
Mar 26, 2025	NPF day	Class I	9:00–21:00	8.4	3.3	09:00–09:35	3.4	09:40–18:00	1.2
Mar 27, 2025	NPF day	Class II	9:00–17:00	15.8	3.6	NA	NA	09:20–17:00	0.6
Mar 28, 2025	NPF day	Class II	9:00–14:00	12.3	2.7	NA	NA	09:20–13:40	2.2
Mar 30, 2025	NPF day	Class II	9:00–11:00	3.7	0.6	09:00–09:35	4.3	09:40–10:55	4.7
Apr 2, 2025	NPF day	Class II	8:30–12:30	7.5	1.2	08:30–09:35	1.7	09:40–12:30	1.5
Apr 6, 2025	NPF day	Class II	8:30–13:00	13.4	1.6	NA	NA	08:30–12:55	1.0
Apr 7, 2025	NPF day	Class II	8:30–12:30	8.6	2.1	08:30–09:00	5.8	09:05–12:25	2.2
Apr 8, 2025	NPF day	Class II	8:30–16:30	9.7	1.8	08:30–09:10	3.9	09:15–16:25	1.0
Apr 9, 2025	NPF day	Class II	9:00–16:00	6.4	3.1	09:00–09:35	3.5	09:40–15:55	1.6
Apr 12, 2025	NPF day	Undefined	9:00–11:00	4.1	2.2	NA	NA	09:20–10:55	8.4
Apr 13, 2025	NPF day	Class II	9:00–16:00	9.9	2.0	09:00–09:40	3.5	09:45–15:55	1.2
Apr 16, 2025	NPF day	Class II	8:30–16:00	11.4	5.6	NA	NA	09:00–15:55	1.3
Apr 17, 2025	NPF day	Class I	8:00–18:00	16.8	6.9	NA	NA	08:30–17:55	1.0

Date	Revised classification	Original growth subgroup	NPF window	Mean $N_{3–25}$ (10^3 # cm^{-3})	Mean $N_{25–100}$ (10^3 # cm^{-3})	$GR_{3–7}$ window	$GR_{3–7}$ (nm h^{-1})	$GR_{7–20}$ window	$GR_{7–20}$ (nm h^{-1})
Apr 18, 2025	NPF day	Undefined	11:00–14:00	5.2	1.4	NA	NA	11:25–13:55	1.6
Apr 19, 2025	NPF day	Class II	8:30–18:00	11.0	4.0	NA	NA	08:50–17:55	1.2
Apr 21, 2025	NPF day	Class I	8:00–21:00	16.0	4.1	08:00–08:30	3.0	08:35–17:55	0.9
Apr 22, 2025	NPF day	Class II	9:00–16:00	9.5	1.4	NA	NA	09:15–15:55	0.5
Oct 15, 2024	Undefined	Undefined	NA	2.0	1.1	07:17–12:57	-0.1	07:02–17:57	0.4
Mar 29, 2025	Undefined	Undefined	NA	2.9	0.6	13:35–14:25	0.7	07:00–17:55	-0.2
Apr 10, 2025	Undefined	Undefined	NA	3.9	0.8	NA	NA	07:00–17:55	-0.1
Apr 11, 2025	Undefined	Undefined	NA	5.2	1.0	NA	NA	07:00–17:45	0.0
Apr 14, 2025	Undefined	Undefined	NA	2.6	1.2	NA	NA	07:05–17:55	0.6
Apr 20, 2025	Undefined	Undefined	NA	4.9	0.9	NA	NA	07:20–17:55	0.4
Oct 21, 2024	Non-Event	Non-Event	NA	2.0	1.1	12:32–13:42	-0.7	07:02–17:57	0.4
Nov 5, 2024	Non-Event	Non-Event	NA	1.0	2.3	07:12–17:57	-0.3	07:02–17:17	0.8
Nov 6, 2024	Non-Event	Non-Event	NA	1.1	2.7	NA	NA	07:02–17:57	-0.4
Mar 31, 2025	Non-Event	Non-Event	NA	0.5	0.4	14:35–17:00	0.1	07:00–17:15	-0.9
Apr 1, 2025	Non-Event	Non-Event	NA	0.2	0.4	13:50–14:25	0.5	14:30–18:00	0.5
Apr 3, 2025	Non-Event	Non-Event	NA	0.7	0.4	07:35–10:55	-0.2	07:00–18:00	-0.2
Apr 4, 2025	Non-Event	Non-Event	NA	0.2	0.4	NA	NA	07:20–18:00	0.0
Apr 5, 2025	Non-Event	Non-Event	NA	0.3	0.6	NA	NA	07:00–17:55	0.2
Apr 15, 2025	Non-Event	Non-Event	NA	0.8	1.0	NA	NA	07:00–17:35	-0.4

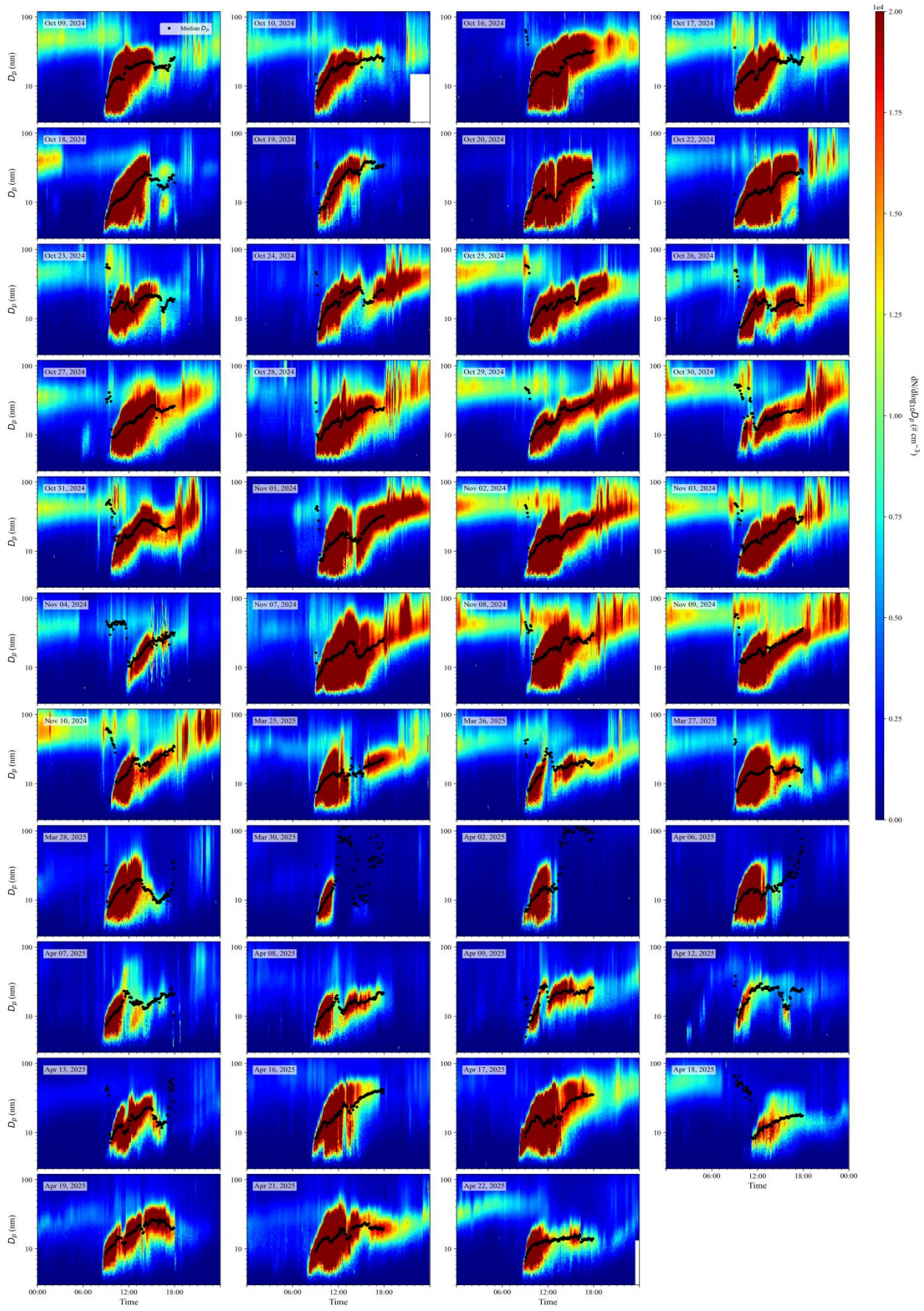

Figure S1: PNSDs for all NPF days. Each panel represents one day. The black dots indicate the median particle diameter.

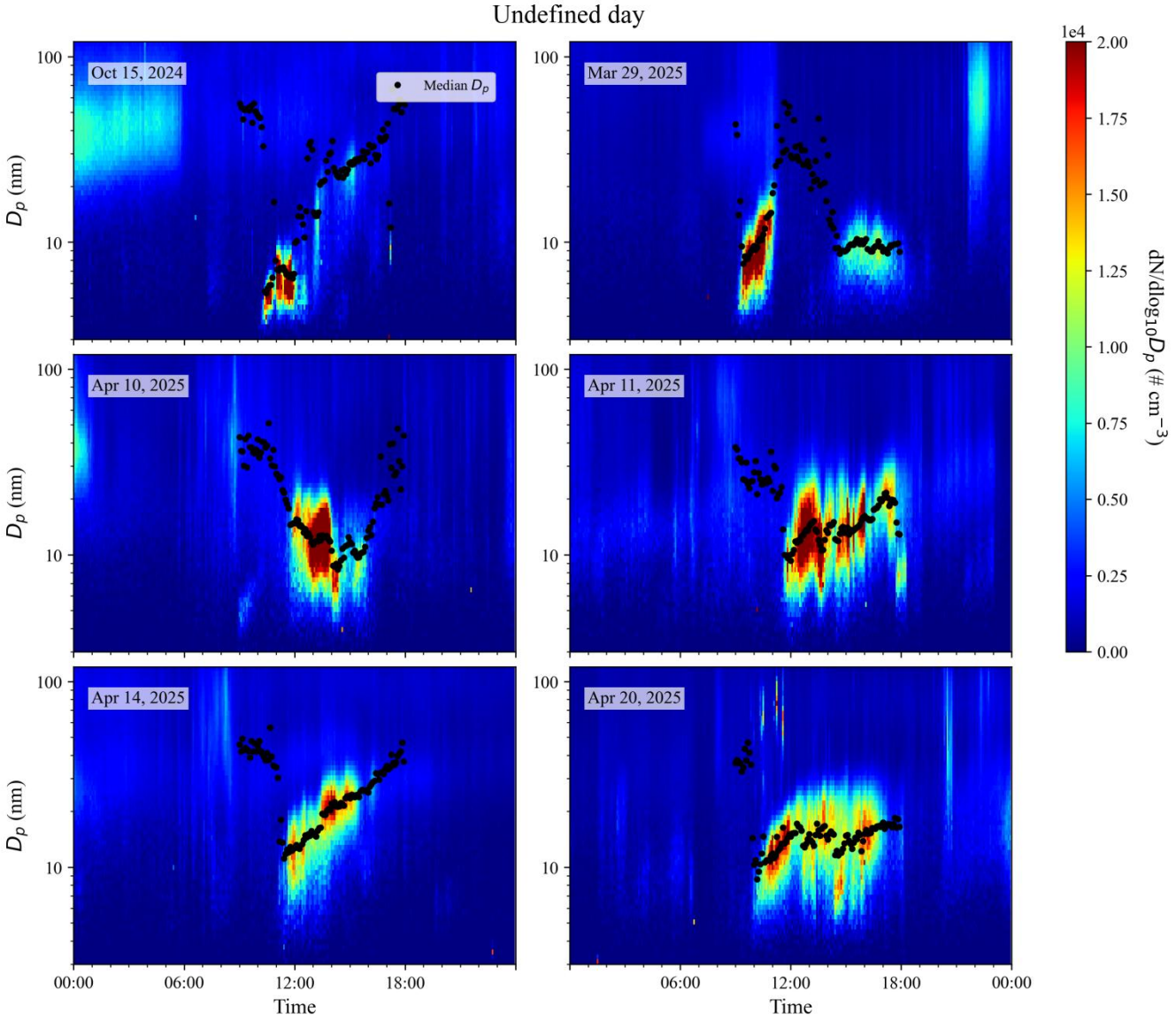

Figure S2: PNSDs for all Undefined days. Each panel represents one day. The black dots indicate the median particle diameter.

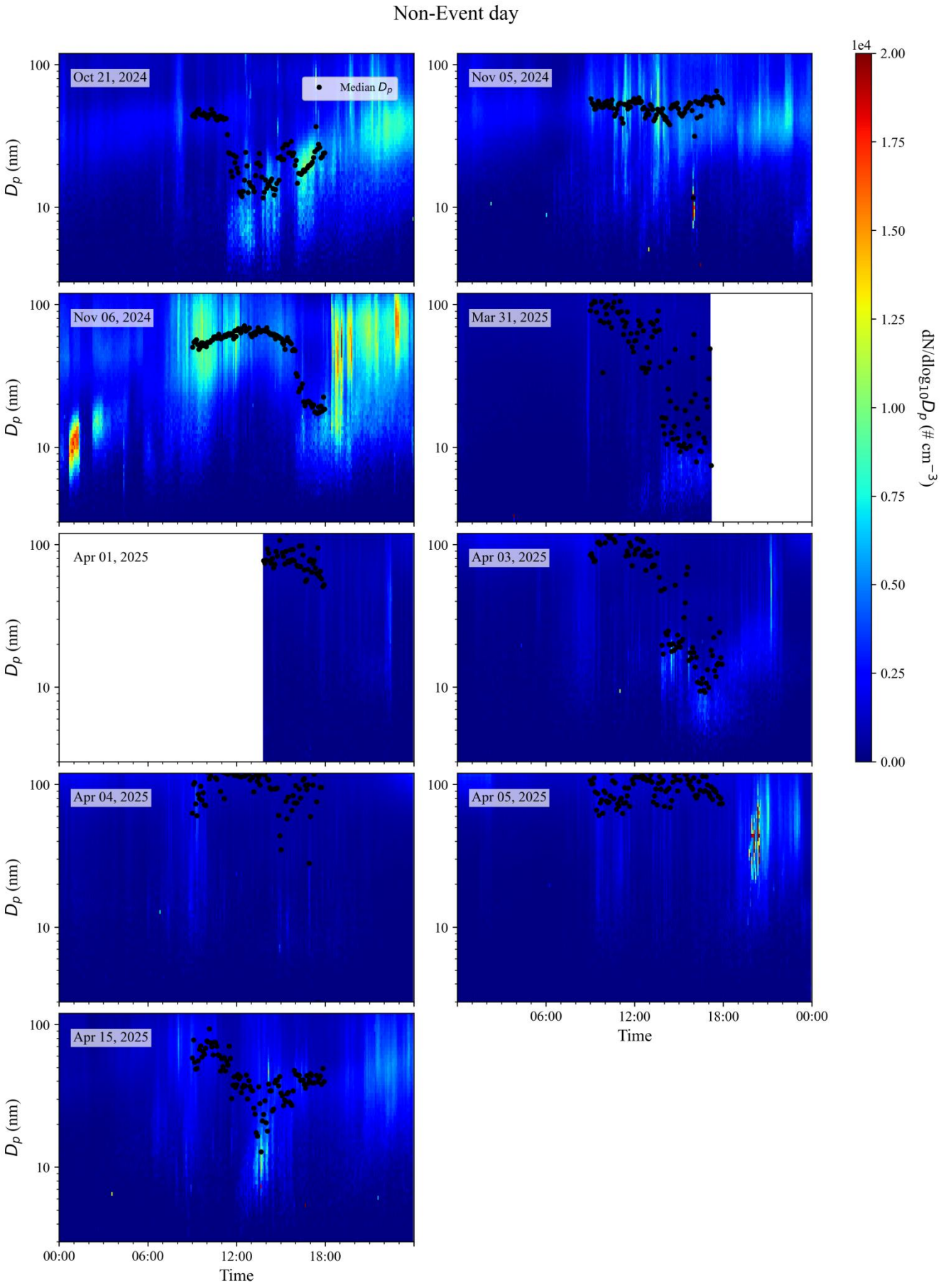

Figure S3: PNSDs for all Non-Event days. Each panel represents one day. The black dots indicate the median particle diameter.

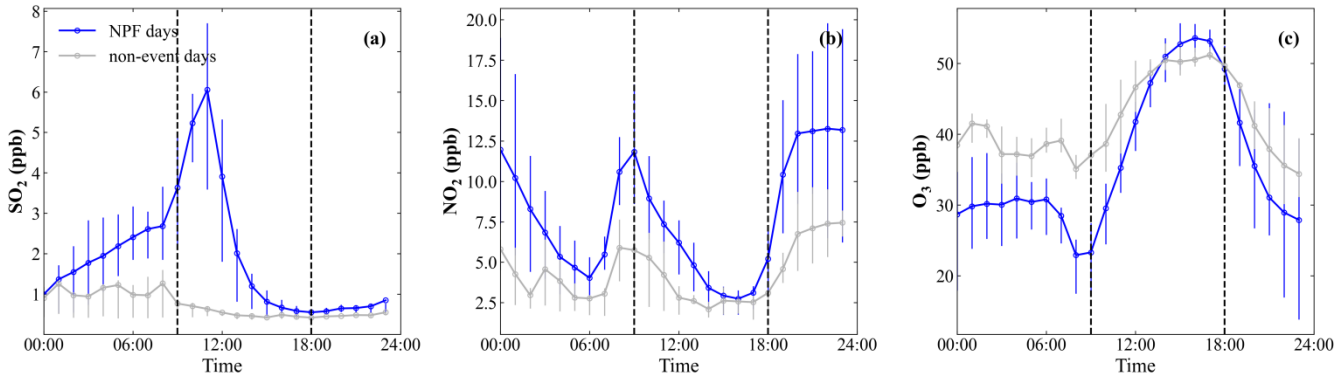

Figure S4: Diurnal variations of (a) SO_2, (b) NO_2, and (c) O_3 during the autumn observation period on NPF days and non-NPF days. The upper and lower bars indicate the 75th and 25th percentiles, respectively, and the markers represent the average values.

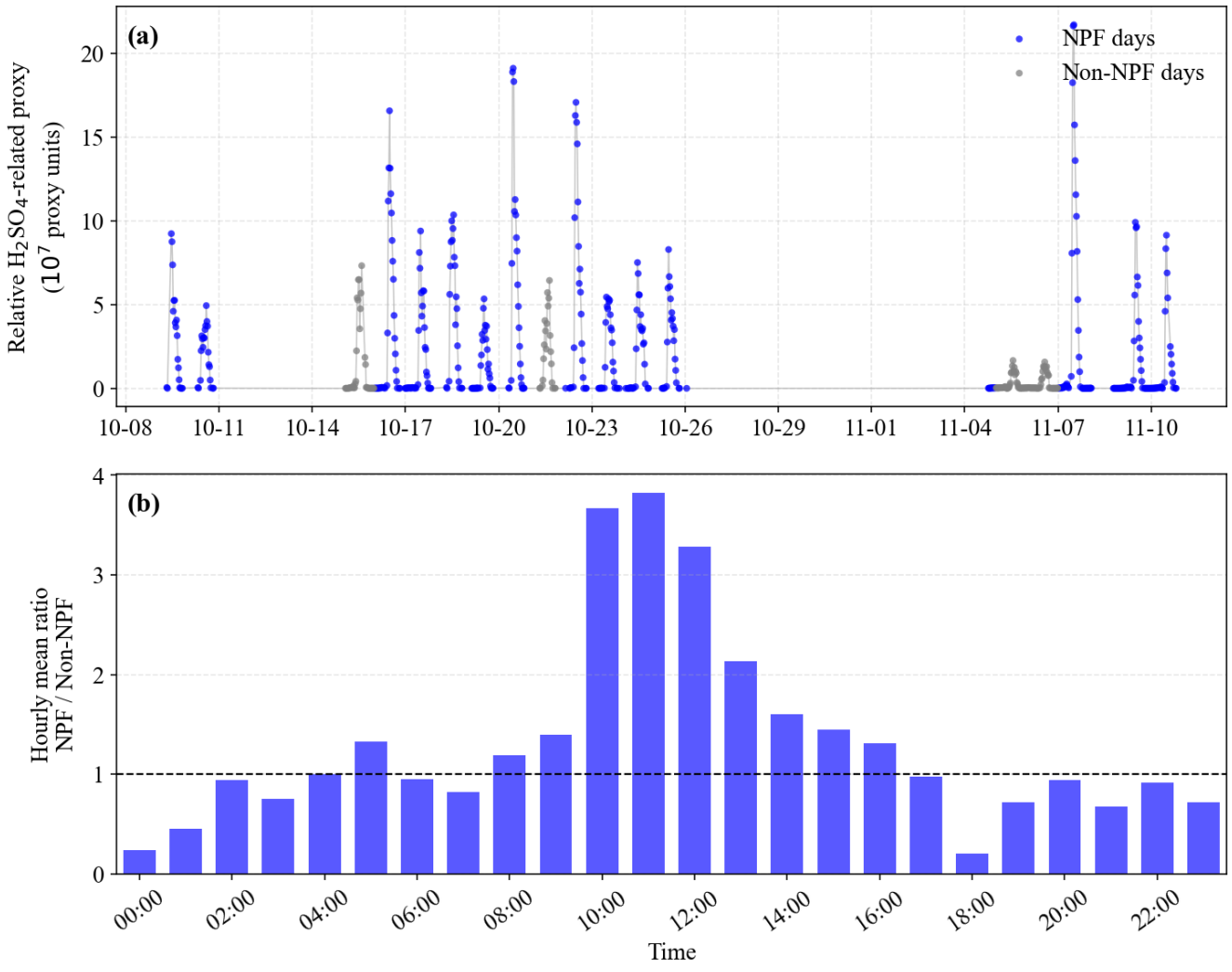

Figure S5: H_2SO_4-related photochemical proxy during periods with available spectral measurements in the autumn observation period. (a) Time series of the 30 min proxy values on NPF and non-NPF days. (b) Ratio of the hourly mean proxy on NPF days to that on non-NPF days.

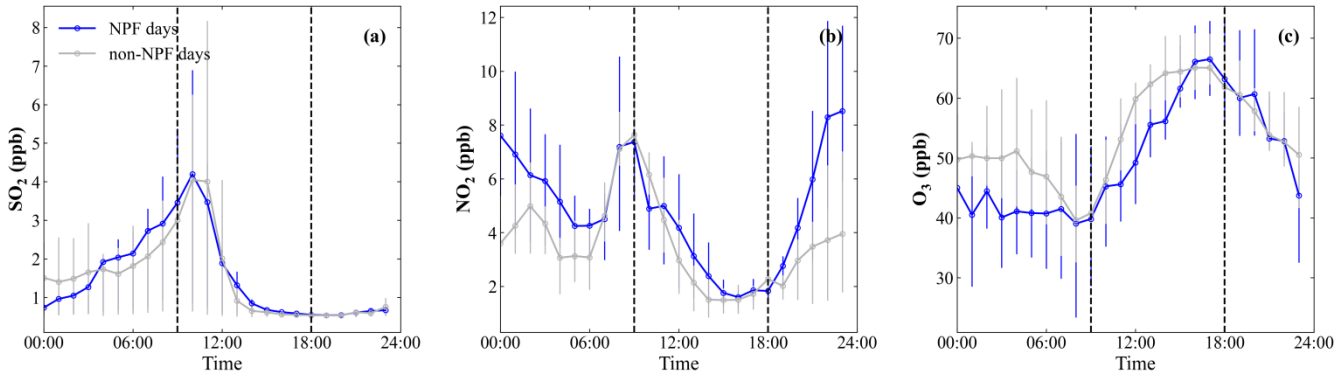

Figure S6: Diurnal variations of (a) SO_2, (b) NO_2, and (c) O_3 during the spring observation period on NPF days and non-NPF days. The upper and lower bars indicate the 75th and 25th percentiles, respectively, and the markers represent the average values.

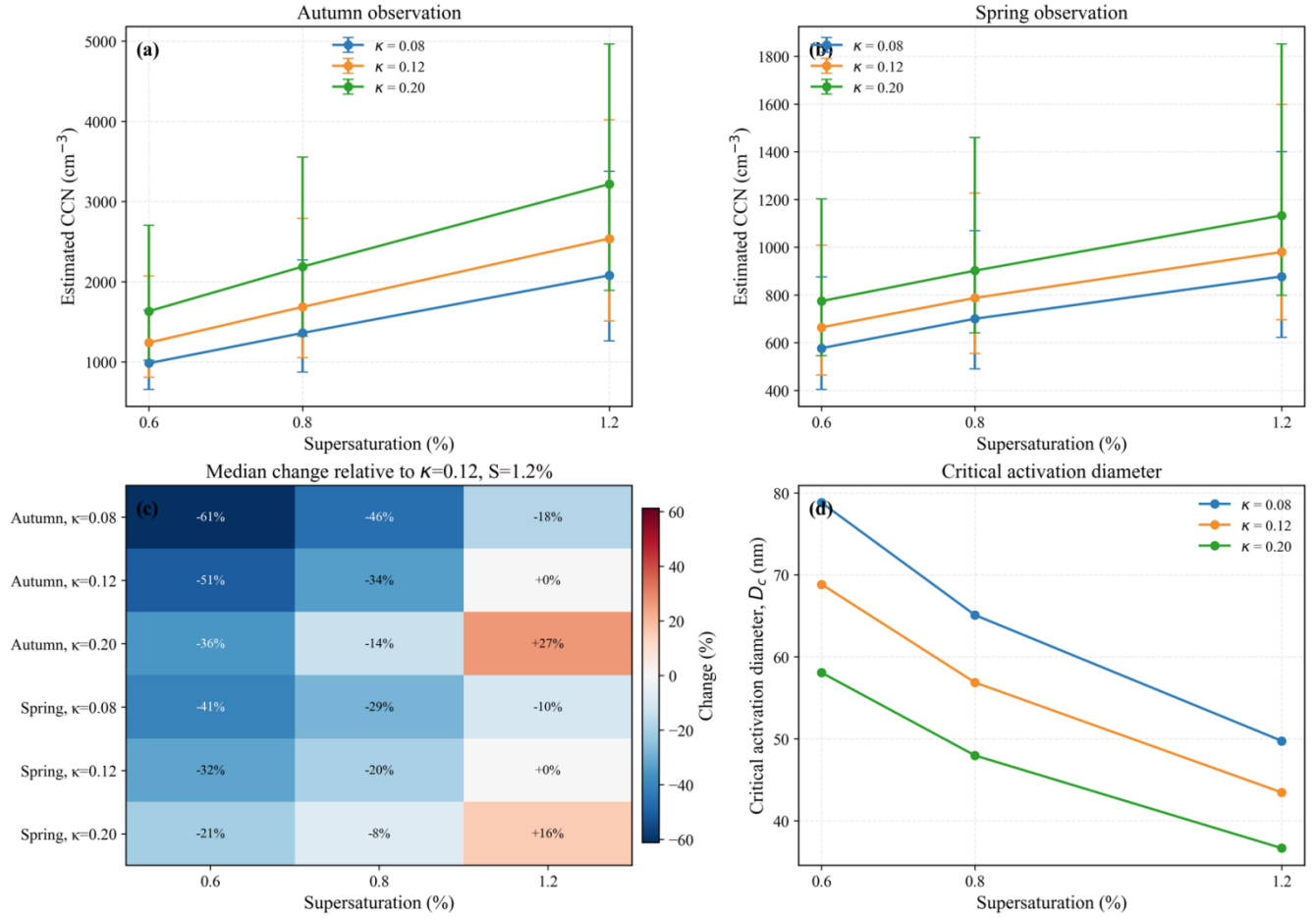

Figure S7. Sensitivity of estimated CCN concentrations and critical activation diameter to the assumed particle hygroscopicity parameter (κ) and supersaturation (S). Panels (a) and (b) show the median estimated CCN concentrations, with error bars representing the interquartile range, under different κ and S assumptions during the autumn and spring observation periods, respectively. Panel (c) shows the percentage change in median CCN relative to the baseline assumptions of κ = 0.12 and S = 1.2 %. Panel (d) shows the corresponding critical activation diameters.

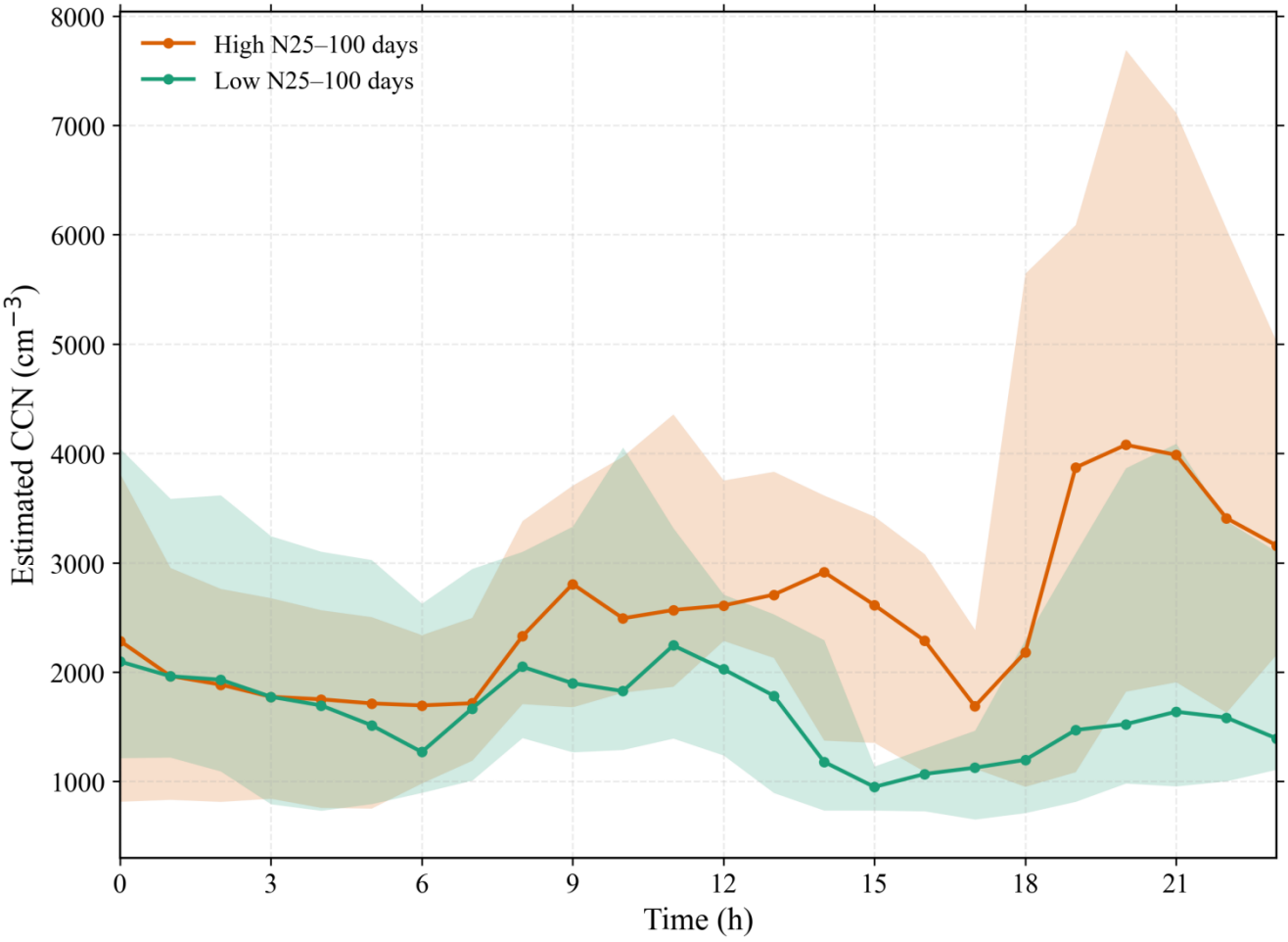

Figure S8. Diurnal variation in estimated CCN concentrations on NPF days with relatively high and low N_{25-100}. Lines and shaded areas represent the medians and interquartile ranges across days, respectively.

References

Dada, L., Ylivinkka, I., Baalbaki, R., Li, C., Guo, Y., Yan, C., Yao, L., Sarnela, N., Jokinen, T., Daellenbach, K. R., Yin, R., Deng, C., Chu, B., Nieminen, T., Wang, Y., Lin, Z., Thakur, R. C., Kontkanen, J., Stolzenburg, D., Sipilä, M., Hussein, T., Paasonen, P., Bianchi, F., Salma, I., Weidinger, T., Pikridas, M., Sciare, J., Jiang, J., Liu, Y., Petäjä, T., Kerminen, V. M., and Kulmala, M.: Sources and sinks driving sulfuric acid concentrations in contrasting environments: implications on proxy calculations, Atmos. Chem. Phys., 20, 11747–11766, 10.5194/acp-20-11747-2020, 2020.

Petäjä, T., Mauldin, I. R. L., Kosciuch, E., McGrath, J., Nieminen, T., Paasonen, P., Boy, M., Adamov, A., Kotiaho, T., and Kulmala, M.: Sulfuric acid and OH concentrations in a boreal forest site, Atmos. Chem. Phys., 9, 7435–7448, 10.5194/acp-9-7435-2009, 2009.

Rohrer, F. and Berresheim, H.: Strong correlation between levels of tropospheric hydroxyl radicals and solar ultraviolet radiation, Nature, 442, 184–187, 10.1038/nature04924, 2006.